# Monitoring single-synapse glutamate release and presynaptic calcium concentration in organised brain tissue

Thomas P. Jensen[1], Kaiyu Zheng[1], Olga Tyurikova[1,2], James P. Reynolds[1], Dmitri A. Rusakov[1]

[1] UCL Institute of Neurology, University College London, Queen Square, London WC1N 3BG, U.K.;

[2] Institute of Neuroscience, University of Nizhny Novgorod, 603950 Nizhny Novgorod, Russia;

Correspondence: Dmitri Rusakov d.rusakov@ucl.ac.uk or Thomas Jensen t.jensen@ucl.ac.uk

## Abstract

Brain function relies in large part on $Ca^{2+}$-dependent release of the excitatory neurotransmitter glutamate from neuronal axons. Establishing the causal relationship between presynaptic $Ca^{2+}$ dynamics and probabilistic glutamate release is therefore a fundamental quest across neurosciences. Its progress, however, has hitherto depended primarily on the exploration of either cultured nerve cells or giant central synapses accessible to direct experimental probing *in situ*. Here we show that combining patch-clamp with time-resolved imaging of $Ca^{2+}$ -sensitive fluorescence lifetime of Oregon Green BAPTA-1 (Tornado-FLIM) enables readout of single spike-evoked presynaptic $Ca^{2+}$ concentration dynamics, with nanomolar sensitivity, in individual neuronal axons in acute brain slices. In parallel, intensity Tornado imaging of a locally expressed extracellular optical glutamate sensor iGluSnFr provides direct monitoring of single-quantum, single-synapse glutamate releases *in situ*. These two methods pave the way for simultaneous registration of presynaptic $Ca^{2+}$ dynamics and transmitter release in an intact brain at the level of individual synapses.

## 1. Introduction

$Ca^{2+}$-dependent, stochastic release of neurotransmitter quanta is a long-recognised, fundamental function of neurons [1]. Monitoring synaptic release events and $Ca^{2+}$ concentration ($[Ca^{2+}]$) dynamics at individual axonal terminals has since provided critical advances in our understanding of brain function [2, 3]. Historically, accurate measurements of axonal $[Ca^{2+}]$ *in situ* have relied on the experimental probing of giant calyceal synapses in acute brain slices. These preparations allow direct experimental access to individual, superficially occurring presynaptic terminals thus enabling whole-cell patch recording combined with ratiometric $Ca^{2+}$ imaging [4-8]. Whilst ratiometric indicators can provide $[Ca^{2+}]$ readout, their use in organised brain tissue is limited by light absorption and scattering, which are strongly wavelength-dependent [9] and thus could affect the ratio of chromatically separated signals. Furthermore, fluorescence signals from small presynaptic boutons of common excitatory synapses typically have the signal-to-noise ratio which is too low to obtain reliable ratiometric measurements. Instead, monitoring presynaptic $[Ca^{2+}]$ dynamics *in situ* has been routinely carried out using fluorescence intensity measures [10-12]. This approach however has low sensitivity to low basal $[Ca^{2+}]$ (<100 nM) and normally requires non-stationary kinetic modelling and various controls to translate recorded fluorescence into $[Ca^{2+}]$ dynamics [13-15].

These complications in large part can be dealt with by using fluorescence lifetime imaging (FLIM) of $Ca^{2+}$ indicators whose fluorescence lifetime is specifically sensitive to free $[Ca^{2+}]$, such as Oregon Green BAPTA-1 (OGB-1) [16-18]. We have recently advanced a two-photon excitation (2PE) FLIM technique which, by optimising photon counting, boosts image acquisition rate hence spatiotemporal resolution of recorded $[Ca^{2+}]$ in neurons and astroglia, *in situ* and *in vivo* by [19]. Here we take this technique one step further, implementing the FLIM scanning mode (Tornado) that enables readout of single action potential-evoked presynaptic $[Ca^{2+}]$ dynamics, with nanomolar sensitivity, in individual small presynaptic boutons in acute brain slices.

As for the monitoring of neurotransmitter release events, for decades it relied on the registration of postsynaptic receptor currents using a patch-clamp technique. An important advance came in the shape of an optical quantal analysis in which successful single-synapse glutamate releases *in situ* are registered by detecting (NMDA receptor-dependent) $Ca^{2+}$ entry in postsynaptic dendritic spines [20-22]. The signal-to-noise ratio in such recordings is however relatively low, the slow NMDA receptor kinetics complicates registration of repetitive releases, and these observations are usually uncoupled from the monitoring of presynaptic $Ca^{2+}$. Another powerful method to track synaptic release has been the presynaptic uptake of fluorescent FM dyes in the course of vesicular exocytosis [23, 24] which could be combined with presynaptic $[Ca^{2+}]$ monitoring [14]. This was further advanced with single-vesicle imaging employing pH-sensitive indicators (pHluorins) targeted to the synaptic vesicle lumen [25, 26]. The use of this potent method *in situ* could be however complicated, mainly because of its stringent requirements to the optical

environment which has to favour reliable signal detection from individual release sites.

Recently, a genetically encoded high-affinity glutamate sensor iGluSnFr has been developed providing robust registration of synaptically evoked glutamate transients in the extracellular space *in situ* [27]. Here we show that combining whole-cell single axon tracing with local iGluSnFr expression enables reliable registration of spike-evoked quantal glutamate release events from individual axonal boutons of principal neurons *in situ*. The approach opens a new window into our quest to understand the principles of synaptic signal integration in the brain.

## 2. Material and Methods

### *2.1. iGluSnFr transduction of hippocampal neurons*

All animal procedures were conducted in accordance with the European Commission Directive (86/609/ EEC) and the United Kingdom Home Office (Scientific Procedures) Act (1986). Young C57BL/6 mice (3 - 4 weeks of age) male and female, were anaesthetised using isoflurane (5% induction, 1.5 - 2.5% v/v). Upon loss of pedal withdrawal reflexes, the animal was secured in a stereotaxic frame (David Kopf Instruments, CA, USA). Perioperative analgesics were administered (subcutaneous buprenorphine, 60 µg $kg^{-1}$) and the scalp was shaved and disinfected using three washes of topical chlorhexidine. A small midline incision was made and the skull was exposed. A craniotomy of approximately 1 - 2 mm diameter was performed over the right hemisphere using a high-speed hand drill (Proxxon, Föhren, Germany), at a site overlying the medial hippocampus. Stereotactic coordinates were 60 % of the anterioposterior distance from bregma to lambda and 2.5 mm lateral to midline. Once exposed, a warmed aCSF variant (cortex buffer; in mM, 125 NaCl, 5 KCl, 10 HEPES, 10 glucose, 2 $CaCl_2$, 2 $MgSO_4$) was applied to the skull and cortical surface throughout the procedure.

Pressure injections of AAV9 *hSyn iGluSnFr* (totalling 0.1 - 1 x $10^{10}$ genomic copies in a volume not exceeding 200 nL, supplied by Penn Vector Core, PA, USA) were carried out using a pulled glass micropipette stereotactically guided to a depth of 1.3 mm beneath the cortical surface, at a rate of approximately 1 nL $sec^{-1}$. The total injection volume was delivered in three steps, reducing depth by 100 µm at each step. Once delivery was completed, pipettes were left in place for 5 minutes before being retracted. The surgical wound was closed with absorbable 7-0 sutures (Ethicon Endo-Surgery GmbH, Norderstedt, Germany) and the animal was left to recover in a heated chamber. Meloxicam (subcutaneous, 1 mg $kg^{-1}$) was subsequently administered once daily for up to two days following surgery. Mice were killed by transcardial perfusion with ice-cold sucrose-enriched slicing medium (in mM, 105 sucrose, 60 NaCl, 2.5 KCl, 1.25 $NaH_2PO_4$, 26 $NaHCO_3$, 15 glucose, 1.3

ascorbic acid, 3 Na pyruvate, 0.5 $CaCl_2$ and 7 $MgCl_2$, saturated with 95% $O_2$ and 5% $CO_2$) after a 2 - 4 week AAV incubation period and acute cortical slices prepared for imaging and electrophysiological recordings as below.

*2.2. Brain slice Preparation*

Acute 350 µm thick hippocampal slices were obtained from either 3-4 week old Sprague-Dawley rats or 5-7 week old C57BL/6 mice, as specified, in full compliance with national guidelines on animal experimentation. Slices were prepared in an ice-cold slicing solution described above, stored in the slicing solution at 34°C for 15 min before being transferred to a submersion chamber for storage in an extracellular solution containing (in mM) NaCl 119, KCl 2.5, $MgSO_4$ 1.3, $NaH_2PO_4$ 1, $NaHCO_3$ 26, $CaCl_2$ 2, glucose 10 (osmolarity adjusted to 295–305 mOsM with glucose). All solutions were continuously bubbled with 95% $O_2$/5% $CO_2$. Slices were allowed to rest for at least 60 min before recordings started.

*2.3 Axon tracing and Tornado scanning in pre-synaptic boutons*

We used a Femtonics Femto3D-RC or Femto2D-FLIM imaging system, integrated with patch-clamp electrophysiology (Femtonics, Budapest) and both linked on the same light path to two femtosecond pulse lasers MaiTai (SpectraPhysics-Newport) with independent shutter and intensity control as previously described [28]. Patch pipettes were prepared with thin walled borosilicate glass capillaries (GC150-TF, Harvard apparatus) with open tip resistances 2.5-3.5 or 3.5-4.5 MOhms for CA3 pyamidal cells or CA1 interneurones respectively. Internal solution contained (in mM) 135 potassium methanesulfonate, 10 HEPES, 10 di-Tris-Phosphocreatine, 4 $MgCl_2$, 4 $Na_2$-ATP, 0.4 Na-GTP (pH adjusted to 7.2 using KOH, osmolarity 290–295), and supplemented with the morphological tracer dye Alexa 594 (50 µM) with addition of Oregon Green BAPTA-1 (300 µM) for FLIM imaging.

Pre-synaptic imaging was carried out using an adaptation of pre-synaptic $Ca^{2+}$ imaging methods previously described [22]. Following break-in 45-60 minutes were allowed for Alexa 594 to equilibrate across the axonal arbour. Axons, identified by their smooth morphology and often torturous trajectory were followed in frame scan mode to their respective targets in CA1. Discrete boutons were identified by criteria previously demonstrated to reliably match synaptophysin labelled punctae [29, 30]. Once identified, spiral shaped (Tornado) line scans of diameter equivalent to the bouton were produced from single points using the MES software (Femtonics). Depending on the bouton size, one spiral scan typically takes 1-1.5 ms, thus providing comprehensive, high-resolution readout of axonal fluorescence.

*2.3. 2PE Tornado-FLIM readout of $Ca^{2+}$ concentration in small axonal boutons.*

Here we identified and patched CA1 *stratum radiatum* interneurons located close to the apical border of the pyramidal cell layer. Axons were followed as above to boutons present in, around or within the pyramidal cell layer and, initially, line scans were carried out with a single action potentials initiated by brief positive voltage steps in voltage clamp mode (Vm holding -70mV). Tornado scan data were recorded by both standard analogue integration in Femtonics MES and in TCSPC in Becker and Hickl SPCM using dual HPM-100 hybrid detectors. Next we used the fast-FLIM analysis procedure described previously [19] to handle individual Tornado scans (also see in [19] the general diagram illustrating the TCSPC data conversion into dynamic [$Ca^{2+}$] changes). Thus, the fast-FLIM linescan data were collected and stored as 5D-tensors (*t,x,y,z,T*) to be analysed with a custom written data analysis software available online (https://github.com/zhengkaiyu/FIMAS).

In the present study, the signal localisation inside the bouton on the submicron scale was not analysed. Thus, present *x,y* and *z* data were summed (averaged) along their respective axes. The data were then summed along the time axis, with bin sizes adequate for the accurate NTC measure to extrapolate [$Ca^{2+}$] from FLIM data (5-10 ms depending on photon counts). In boutons close to the slice surface where photon counts were relatively high the temporal binning could be short enough to enable recording of individual [$Ca^{2+}$] transients resulting from single action potentials. In boutons deeper within the slice multiple trials were summed to produce photon counts high enough to accurately determine dynamics of single action potential [$Ca^{2+}$] transients.

### *2.4. Presynaptic imaging of quantal glutamate release*

Cells were first identified as iGluSnFr expressing using two-photon imaging at 910 nm and patched in whole cell mode as above with the omission of OGB-1 from the internal solution. Using Alexa 594 fluorescence (excited at 800 nm) the axons were then traced into the CA1 region (up to 500 μm from the patched cell body, inside *stratum radiatum*). Again, for the fast imaging of action-potential mediated iGluSnFr transients a Tornado (spiral shaped) scan line was placed over the bouton of interest (described further in the text) which was then scanned at a sampling frequency of ~500 Hz with excitation at 910 nm. Following a baseline period, a pair of action potentials were generated by brief positive voltage steps in voltage clamp mode (Vm holding -70mV), with an interval of 50 ms. Recorded Tornado linescan data were analysed using custom written data analysis routines in MATLAB 2016a (Mathworks) and traces expressed as ΔF/F.

## 3. Results

### *3.1. OGB-1 Tornado-FLIM readout of presynaptic [$Ca^{2+}$] dynamics in small axonal boutons of central neurons in situ*

We reported earlier that a ratiometric version of FLIM applied to OGB-1 could provide reliable readout of intracellular [$Ca^{2+}$] in astroglia and neurons *in situ*, including [$Ca^{2+}$] dynamics in neuronal dendrites [19]. Here, we used a different microscope setup (Femtonics) and therefore re-calibrated OGB-1 lifetime for FLIM measurements of [$Ca^{2+}$] using standard Ca2+-clamped probes as described before [19], to account for any possible instrumental bias (Fig. 1A-B). Our initial attempts to apply a FLIM-based approach to small axonal boutons were unsuccessful, mainly due to the small imaged volume (hence low photon counts) and the photo-bleaching and photo-toxicity concomitants pertinent to repeated line-scanning. Both frame-scanning and line-scanning modes appeared to produce unsatisfactory temporal resolution and signal-to-noise ratios in the case of axonal recordings *in situ*.

These drawbacks arise mainly because standard scanning modes provides a pixel-sampling sequence which deviates substantially from the circular geometry of small axonal boutons and is limited by the finite scanning frequency. We therefore modified our imaging procedures to enable spiral ('Tornado') scanning which provides circular pixel sampling and thus records the signal spatiotemporal dynamics more favourably (Fig. 1C). Another important advantage of these experiments was the dual detector equipped with analogue and photon-counting outputs. This enabled prompt visualisation of the bouton of interest using fluorescence intensity (in the Alexa channel) to correct for any focus drift while registering FLIM readout. Equipped with these methods we were able to obtain reliable Tornado-FLIM readout of presynaptic [$Ca^{2+}$] concentration dynamics in small axonal boutons in response to individual action potentials (Fig. 1E). These direct [$Ca^{2+}$] measurements suggest a very low resting axonal [$Ca^{2+}$] (~20 nM range), which sharply increases upon spike arrival. This post-spike [$Ca^{2+}$] elevation (to 200-300 nM) represents [$Ca^{2+}$] equilibrated across the bouton ~10 ms following the initial, very rapid [$Ca^{2+}$] transient: the latter is necessarily masked in these measurements because FLIM readout requires at least several millisecond exposure to accumulate the required number of photon counts [19].

It is also well known that [$Ca^{2+}$] measurements with $Ca^{2+}$ indicators involve significant exogenous $Ca^{2+}$ buffering and thus potentially distort the endogenous [$Ca^{2+}$] transients, as we and others have previously demonstrated in various synaptic scenarios [11, 13, 31-33]. However, understanding the live relationship between the recorded presynaptic [$Ca^{2+}$] dynamics *in situ* - whether or not it is affected by the experimental protocol - and neurotransmitter release remains an important challenge in neuroscience. Reassuringly, steady-state [$Ca^{2+}$] in neurons and astroglia does not seem to be affected by standard $Ca^{2+}$ indicators [19], and the endogenous [$Ca^{2+}$] dynamics on a fast (sub-millisecond) scale can be theoretically recovered from the $Ca^{2+}$ -dependent fluorescence intensity data [15, 31, 34, 35] using key experimental constraints provided by the FLIM [$Ca^{2+}$] readout.

*3.2. Imaging quantal glutamate release from individual CA3-CA1 pre-synaptic boutons using the glutamate sensor iGluSnFr*

In order to overcome some of the limitations pertinent to the existing glutamate release monitoring methods (Introduction) we employed the recently developed genetically encoded glutamate sensor [27] expressing it in the hippocampal neuropil through viral transfection (Materials and Methods). We thus observed that neuronal iGluSnFr expression was present across the dorsal-ventral axis of the hippocampus and that the location of expression was dependent on the position from the injection site. Close to the injection site in dorsal CA1, pyramidal cells were densely labelled as would be expected. In slices further toward the ventral hippocampus some sparser expression in CA3 pyramidal cells and dentate granule cells was observed with little or no expression in CA1 (Fig. 2A). We took advantage of this lack of dendritic iGluSnFr expression in CA1 to facilitate visualisation of iGluSnFr expressing CA3 axons passing through the CA1 *stratum radiatum*.

Thus, to associate glutamate release with individual identifiable axonal release sites, we held a CA3 pyramidal cell in whole-cell mode, filled it in with the bright morphological tracer Alexa Fluor 594, and traced its axon from the perisomatic location for several hundred microns, into the CA1 *stratum radiatum* (Fig. 2A). The axonal boutons forming CA3-CA1 excitatory synapses could be readily identified in the (red) Alexa emission channel, as described earlier [22, 30]. In the chromatically separated (green) iGluSnFr channel, we thus were able to image individual action potential-induced quantal glutamate release, again, using the Tornado-scanning mode (Fig. 2B) to improve the signal-to-noise ratio. Another important advantage of this acquisition mode compared to line scan was that it would not miss the signal origin site (and hence its largest magnitude). Strikingly, because no appreciable spontaneous synaptic activity was expected in the quiescent tissue here and because the iGluSnFr signal disappeared within ~1 μm from the bouton, the approach could clearly relate stochastic quantal release events to the imaged axonal specialisations (Fig. 2C). This method therefore provides a reliable tool to monitor single-synapse glutamate release in response to individual action potentials in organised brain tissue, with high signal-to-noise ratios.

## 4. Discussion

In this study we advanced and implemented two imaging methods aiming at the high-resolution monitoring of individual synaptic events *in situ*. Our first objective was to enable 'direct' readout of presynaptic [$Ca^{2+}$] dynamics in small axonal boutons representing a common type of excitatory cortical synapses. To achieve that, we set out to register the $Ca^{2+}$-sensitive fluorescence kinetics of the high affinity $Ca^{2+}$ indicator OGB-1. The FLIM method is based on collecting the timing of individual emitted photons through thousands cycles of light emission triggered by very brief (femtosecond range) laser pulses. It thus involves data collection and analyses on a

pixel-by-pixel basis throughout the region of interest. Because of that complex procedure, FLIM usually imposes severe limitations on the temporal resolution of imaging also requiring significant exposure of live preparations to laser light. To improve these aspects of FLIM we earlier advanced a simple ratiometric approach, in which the OGB-1 fluorescence decay kinetic is represented, in words, by its area-under-the-curve related to the peak amplitude [36]. This approach has significantly reduced the number of photon counts required to establish the correspondence between the OGB-1 lifetime kinetics and the pre-calibrated [$Ca^{2+}$] value, thus boosting spatiotemporal resolution of FLIM. However, when applied in standard scanning mode (frame- or line-scan) to monitor [$Ca^{2+}$] dynamics in thin neuronal axons and their small boutons, it still produced unsatisfactory signal-to-noise ratios. In the present study therefore we combined FLIM analyses with Tornado (circular spiral) laser scanning mode to collect photons from the central-symmetric region of interest, such as small axonal boutons. Tornado-FLIM enabled us to obtain 'direct' presynaptic [$Ca^{2+}$] readout in axons of central interneurons *in situ*, with the combined [$Ca^{2+}$] sensitivity and temporal resolution unattainable previously.

Whilst this method can, in principle, provide a 1 kHz or higher data FLIM acquisition rate, the axonal [$Ca^{2+}$] registration bottleneck depends on several factors. Firstly, the minimum number of photon counts. In the case of dendritic recordings, fast-FLIM line scan could provide up to 100 Hz acquisition of internal [$Ca^{2+}$] values, as shown earlier [19]. However, the much smaller cytosolic volume of axons (hence lower numbers of fluorophore molecules) requires the correspondingly longer sampling window thus resulting in slower readout imposing an 'averaging' filter of at least several milliseconds. Finally, diffusion equilibration of intracellular $Ca^{2+}$ with local $Ca^{2+}$ buffers and indicators in the microscopic region of interest may take several milliseconds, thus imposing another omnipresent spatiotemporal filter on [$Ca^{2+}$] monitoring outcome.

Our second objective was to develop a reliable method of detecting quantal release of glutamate at individual identified cortical synapses *in situ*. In the past, this was achieved through postsynaptic receptor current recordings, optical quantal analysis ($Ca^{2+}$ entry events in postsynaptic dendritic spines), or the FM dye- or pHluorin-based registration of the presynaptic release kinetics. These methods drove fundamental advances in our understanding of the synaptic machinery yet they had their limitations. In large part, these limitations were related to the low signal-to-noise ratio or the method's applicability in organised brain tissue (see Introduction). Here, we took advantage of the newly developed glutamate sensor iGluSnFr, expressed it in the hippocampal area CA1 using viral transfection and combined it with single-axon tracing in individual CA3 pyramidal cells held in whole-cell mode. Chromatic separation of the glutamate sensor channel and the morphological tracer channel enabled us to relate individual identifiable axonal boutons (forming CA3-CA1 synapses) to individual action potential-evoked release events. The immediate experimental potential of this approach is simultaneous monitoring of release from

multiple boutons with the possibility to probe mechanisms of action potential generation and propagation in axons. The method also provides favourable conditions for correlative structure-function studies including post-hoc EM analyses.

At present, the overlapping emission spectra of OGB-1 and iGluSnFr make it difficult to combine the two techniques, the FLIM-based presynaptic [$Ca^{2+}$] readout and the one-synapse glutamate release detection, in one experiment. However, new $Ca^{2+}$ indicators are emerging which appear to have a [$Ca^{2+}$] sensitive fluorescence lifetime while working in the red spectral region [37]. Because the lifetime of red morphological tracers such as Alexa is not sensitive to [$Ca^{2+}$], the two-red-dye combination should in principle enable the experimental arrangement in which stochastic properties of glutamate release could be directly related to the dynamics of presynaptic $Ca^{2+}$ at individual cortical synapses *in situ*.

## References


[1] B. Katz, R. Miledi, The role of calcium in neuromuscular facilitation, J. Physiol., 195 (1968) 481-492.

[2] B.L. Sabatini, W.G. Regehr, Optical measurement of presynaptic calcium currents, Biophys J, 74 (1998) 1549-1563.

[3] R. Schneggenburger, E. Neher, Intracellular calcium dependence of transmitter release rates at a fast central synapse, Nature, 406 (2000) 889-893.

[4] I.D. Forsythe, Direct patch recording from identified presynaptic terminals mediating glutamatergic EPSCs in the rat CNS in vitro, J. Physiol., 479 (1994) 381-387.

[5] T. Takahashi, I.D. Forsythe, T. Tsujimoto, M. Barnes-Davies, K. Onodera, Presynaptic calcium current modulation by a metabotropic glutamate receptor, Science, 274 (1996) 594-597.

[6] J.H. Bollmann, B. Sakmann, Control of synaptic strength and timing by the release-site Ca2+ signal, Nat Neurosci, 8 (2005) 426-434.

[7] J. Sun, Z.P. Pang, D. Qin, A.T. Fahim, R. Adachi, T.C. Sudhof, A dual-Ca2+-sensor model for neurotransmitter release in a central synapse, Nature, 450 (2007) 676-U674.

[8] G.B. Awatramani, G.D. Price, L.O. Trussell, Modulation of transmitter release by presynaptic resting potential and background calcium levels, Neuron, 48 (2005) 109-121.

[9] M. Oheim, E. Beaurepaire, E. Chaigneau, J. Mertz, S. Charpak, Two-photon microscopy in brain tissue: parameters influencing the imaging depth, J Neurosci Methods, 111 (2001) 29-37.

[10] M. Maravall, Z.F. Mainen, B.L. Sabatini, K. Svoboda, Estimating intracellular calcium concentrations and buffering without wavelength ratioing, Biophys J, 78 (2000) 2655-2667.

[11] A.C. Kreitzer, K.R. Gee, E.A. Archer, W.G. Regehr, Monitoring presynaptic calcium dynamics in projection fibers by in vivo loading of a novel calcium indicator, Neuron, 27 (2000) 25-32.

[12] C. Grienberger, A. Konnerth, Imaging Calcium in Neurons, Neuron, 73 (2012) 862-885.

[13] R. Scott, D.A. Rusakov, Main determinants of presynaptic $Ca^{2+}$ dynamics at individual mossy fiber-CA3 pyramidal cell synapses, J. Neurosci., 26 (2006) 7071-7081.

[14] Y.S. Ermolyuk, F.G. Alder, C. Henneberger, D.A. Rusakov, D.M. Kullmann, K.E. Volynski, Independent regulation of basal neurotransmitter release efficacy by variable $Ca^{2+}$ influx and bouton size at small central synapses, PLoS Biol, 10 (2012) e1001396.

[15] N.P. Vyleta, P. Jonas, Loose coupling between Ca2+ channels and release sensors at a plastic hippocampal synapse, Science, 343 (2014) 665-670.

[16] C.D. Wilms, J. Eilers, Photo-physical properties of Ca2+-indicator dyes suitable for two-photon fluorescence-lifetime recordings, J Microsc, 225 (2007) 209-213.

[17] C.D. Wilms, H. Schmidt, J. Eilers, Quantitative two-photon Ca2+ imaging via fluorescence lifetime analysis, Cell Calcium, 40 (2006) 73-79.

[18] K.V. Kuchibhotla, C.R. Lattarulo, B.T. Hyman, B.J. Bacskai, Synchronous hyperactivity and intercellular calcium waves in astrocytes in Alzheimer mice, Science, 323 (2009) 1211-1215.

[19] K. Zheng, L. Bard, J.P. Reynolds, T.P. Jensen, A.V. Gourine, D.A. Rusakov, Time-resolved imaging reveals heterogeneous landscapes of nanomolar $Ca^{2+}$ in neurons and astroglia, Neuron, 88 (2015) 277–288.

[20] N.J. Emptage, C.A. Reid, A. Fine, T.V. Bliss, Optical quantal analysis reveals a presynaptic component of LTP at hippocampal Schaffer-associational synapses, Neuron, 38 (2003) 797-804.

[21] T.G. Oertner, B.L. Sabatini, E.A. Nimchinsky, K. Svoboda, Facilitation at single synapses probed with optical quantal analysis, Nature Neurosci., 5 (2002) 657-664.

[22] S. Sylantyev, T.P. Jensen, R.A. Ross, D.A. Rusakov, Cannabinoid- and lysophosphatidylinositol-sensitive receptor GPR55 boosts neurotransmitter release at central synapses, Proc Natl Acad Sci U S A, 110 (2013) 5193-5198.

[23] V.N. Murthy, T.J. Sejnowski, C.F. Stevens, Heterogeneous release properties of visualized individual hippocampal synapses, Neuron, 18 (1997) 599-612.

[24] T.A. Ryan, H. Reuter, S.J. Smith, Optical detection of a quantal presynaptic membrane turnover, Nature, 388 (1997) 478-482.

[25] S. Sankaranarayanan, T.A. Ryan, Real-time measurements of vesicle-SNARE recycling in synapses of the central nervous system, Nature Cell Biology, 2 (2000) 197-204.

[26] J. Balaji, T.A. Ryan, Single-vesicle imaging reveals that synaptic vesicle exocytosis and endocytosis are coupled by a single stochastic mode, Proc. Natl. Acad. Sci. USA, 104 (2007) 20576-20581.

[27] J.S. Marvin, B.G. Borghuis, L. Tian, J. Cichon, M.T. Harnett, J. Akerboom, A. Gordus, S.L. Renninger, T.W. Chen, C.I. Bargmann, M.B. Orger, E.R. Schreiter, J.B. Demb, W.B. Gan, S.A. Hires, L.L. Looger, An optimized fluorescent probe for visualizing glutamate neurotransmission, Nature Methods, 10 (2013) 162-170.

[28] K. Boddum, T.P. Jensen, V. Magloire, U. Kristiansen, D.A. Rusakov, I. Pavlov, M.C. Walker, Astrocytic GABA transporter activity modulates excitatory neurotransmission, Nat Commun, 7 (2016) 13572.

[29] N.J. Emptage, C.A. Reid, A. Fine, Calcium stores in hippocampal synaptic boutons mediate short-term plasticity, store-operated Ca2+ entry, and spontaneous transmitter release, Neuron, 29 (2001) 197-208.

[30] D.A. Rusakov, A. Fine, Extracellular $Ca^{2+}$ depletion contributes to fast activity-dependent modulation of synaptic transmission in the brain, Neuron, 37 (2003) 287-297.

[31] D.W. Tank, W.G. Regehr, K.R. Delaney, A quantitative analysis of presynaptic calcium dynamics that contribute to short-term enhancement, J. Neurosci., 15 (1995) 7940-7952.

[32] D.A. DiGregorio, A. Peskoff, J.L. Vergara, Measurement of action potential-induced presynaptic calcium domains at a cultured neuromuscular junction, J. Neurosci., 19 (1999) 7846-7859.

[33] Y.S. Ermolyuk, F.G. Alder, R. Surges, I.Y. Pavlov, Y. Timofeeva, D.M. Kullmann, K.E. Volynski, Differential triggering of spontaneous glutamate release by P/Q-, N- and R-type $Ca^{2+}$ channels, Nat Neurosci, 16 (2013) 1754-1763.

[34] H.J. Koester, B. Sakmann, Calcium dynamics associated with action potentials in single nerve terminals of pyramidal cells in layer 2/3 of the young rat neocortex, J. Physiol., 529 (2000) 625-646.

[35] B.K. Vanselow, B.U. Keller, Calcium dynamics and buffering in oculomotor neurones from mouse that are particularly resistant during amyotrophic lateral sclerosis (ALS)-related motoneurone disease, J. Physiol., 525 (2000) 433-445.

[36] K. Zheng, D.A. Rusakov, Efficient integration of synaptic events by NMDA receptors in three-dimensional neuropil, Biophys J, 108 (2015) 2457-2464.

[37] M. Collot, C. Loukou, A.V. Yakovlev, C.D. Wilms, D. Li, A. Evrard, A. Zamaleeva, L. Bourdieu, J.F. Leger, N. Ropert, J. Eilers, M. Oheim, A. Feltz, J.M. Mallet, Calcium rubies: a family of red-emitting functionalizable indicators suitable for two-photon Ca2+ imaging, J Am Chem Soc, 134 (2012) 14923-14931.

## Acknowledgments

This work was supported by the Wellcome Trust Principal Fellowship (101896), European Research Council Advanced Grant (323113-NETSIGNAL), Russian Science Foundation grant (15-14-30000, Fig. 1AB data), FP7 ITN (606950 EXTRABRAIN), the Medical Research Council (22448).

## Author Contributions

T.P.J., K.Z. and D.A.R. designed the experiments; T.P.J. carried out patch-clamp and imaging experiments in neurons; K.Z. adapted FLIM methods and carried out FLIM analyses; J.R. carried out viral transfection studies; O.T. performed FLIM calibration; T.P.J. and D.A.R. wrote the study which was subsequently contributed to by all the authors.

## Figure legend

**Figure 1.** Two-photon excitation FLIM-based monitoring of intracellular [$Ca^{2+}$] in small axonal boutons in cortical neurons *in situ*.

A, Fluorescence time course of OGB-1 in calibrated solutions of clamped [$Ca^{2+}$], as indicated, in response to a ~200 fs laser pulse, for the optical setup in question. Instrument response (~200 ps half-width) is not subtracted, kinetics shown normalised against peak value (arrow); grey area, area-under-the-curve integration time window in the FLIM calibration protocol.

B, Resultant calibration function depicting normalised total photon count (ratiometric measure) against [$Ca^{2+}$]; see [19] for detail.

C, Diagram depicting some advantages of Tornado scanning over standard frame scanning in imaging axonal boutons (depicted by grey shape). *Left*: An *x-y* frame scan containing *n* lines takes $T = n / f$ where *f* is the scanning frequency. *Right:* In Tornado mode, the entire bouton fluorescence can be sampled over $T = 1/ f$ period (from central point to the tip; in similar pixel settings). Red arrow spans illustrate that registering some (diametrically opposite) areas of the bouton could be separated by $T = n / f$ interval in frame scan mode whereas such separation is always $<< 1 / f$ in the Tornado scan.

D, Tracing small axonal boutons of a CA1 interneuron patched in whole-cell (Alexa channel, $\lambda_x^{2p}$ = 800 nm). Left panel: axonal arborisations traced in area CA1; 180 µm deep 70-section z-stack average (inset, low magnification, patch-pipette shown); dotted rectangle, region of interest (ROI). Right panel: the ROI at high magnification featuring two presynaptic boutons (b1 and b2); spirals illustrate Tornado scanning mode centred at the bouton centroid, as shown by arrows.

E, OGB-1 Tornado-FLIM readout of presynaptic axonal [$Ca^{2+}$] in response to a single action potential (grey, examples of individual recordings; black, average; $\lambda_x^{2p}$ = 800 nm) in boutons b1 and b2, depicted in C, as indicated. Note that the initial rapid [$Ca^{2+}$] transient post-spike (sub-millisecond to millisecond range) is necessarily masked by the temporal filtering due to the minimal FLIM data acquisition time (at least several milliseconds).

**Figure 2.** Monitoring single-spike evoked quantal release of glutamate from individual traced presynaptic axonal boutons of Schaffer collaterals in area CA1.

A, Whole-cell patched CA3 pyramidal cell (red) with the axon traced into the area CA1 (arrows; Alexa channel, $\lambda_x^{2p}$ = 800 nm); dotted rectangle, region of interest (ROI)

B, Right image panel: ROI from A depicting three identifiable axonal boutons; Tornado scanning pattern shown placed in the middle of one bouton, with reference rotational angles 0 and 180$^{o}$ depicted. Left panel: Tornado scan (vertical axis, rotation angles) showing iGluSnFr fluorescence single-trial time course in response to two action potentials (upper trace, escape current recorded at the soma).

C, Examples of the iGluSnFr fluorescence time course ($\lambda_x^{2p}$ = 910 nm) evoked by two spikes generated at the soma (held in whole-cell voltage-clamp) as in B, showing four typical scenarios of probabilistic glutamate releases from the bouton under study (0, failure; 1, success), as indicated.

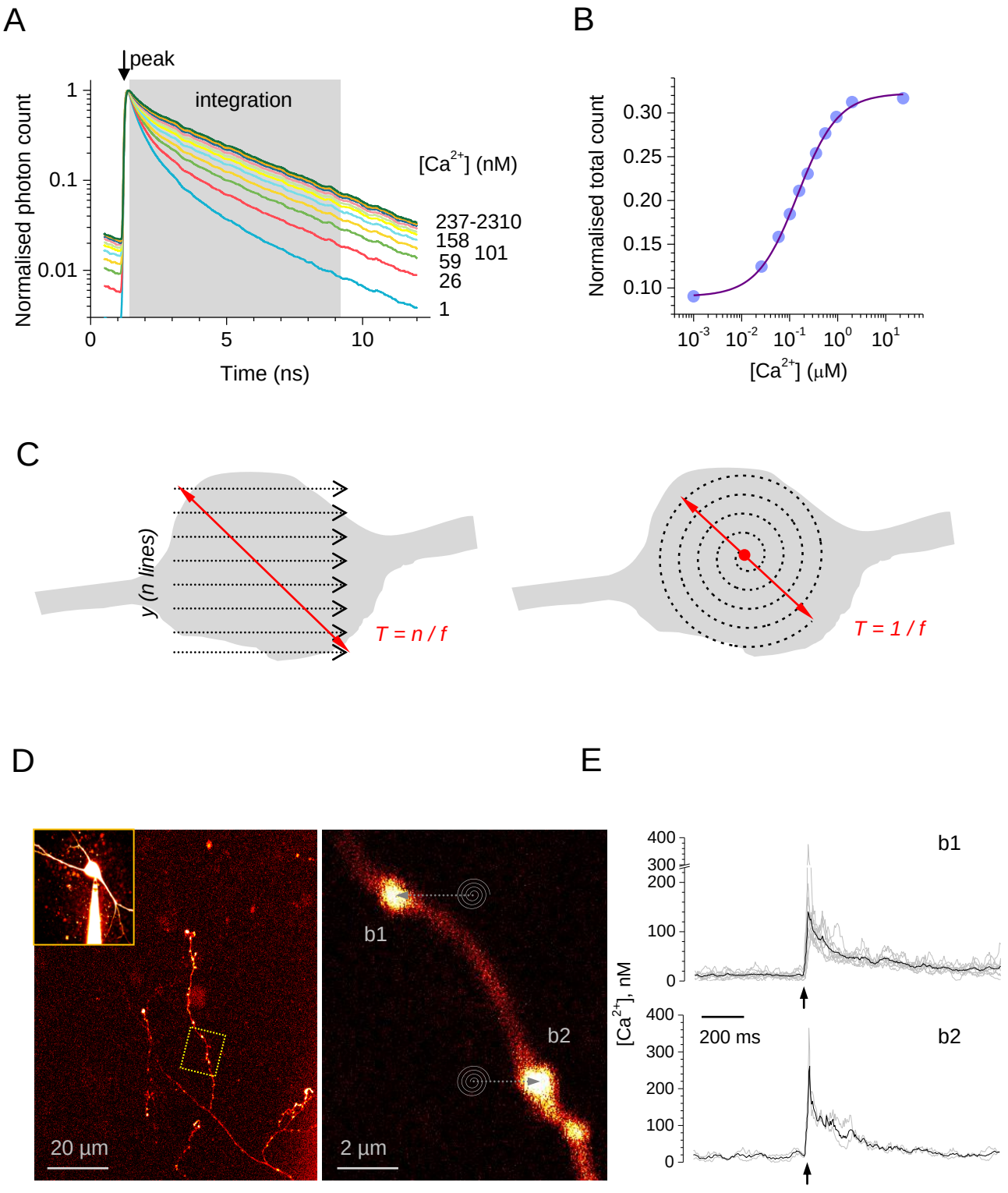
A
peak
integration
Normalised photon count
1
0.1
0.01
0
5
10
Time (ns)
[Ca2+] (nM)
237-2310
158
101
59
26
1
B
Normalised total count
0.30
0.25
0.20
0.15
0.10
10-3
10-2
10-1
100
101
[Ca2+] (μM)
C
y (n lines)
T = n / f
T = 1 / f
D
20 μm
b1
b2
2 μm
E
400
300
200
100
0
[Ca2+], nM
b1
200 ms
b2

Figure 1

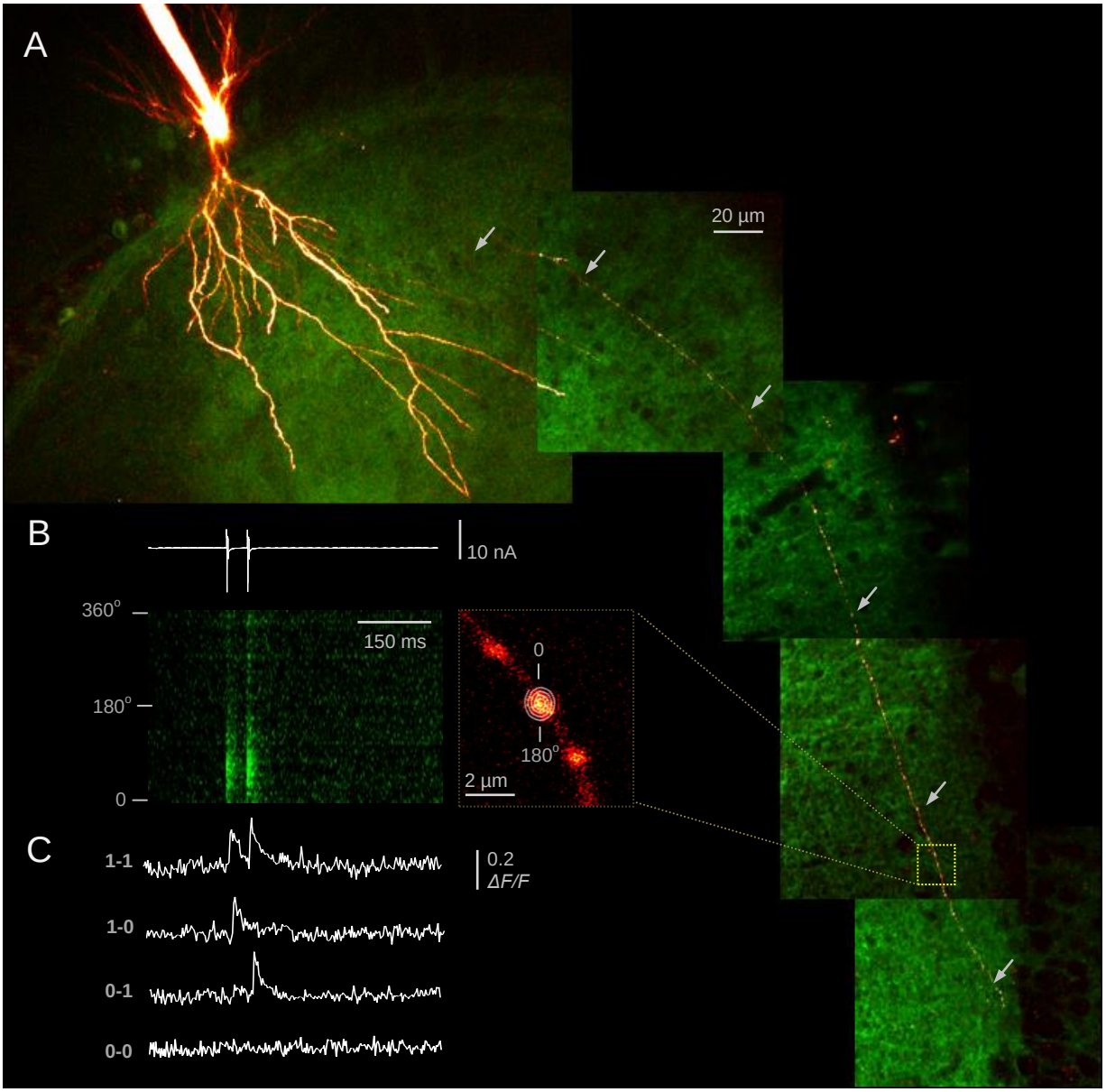


Figure 2